




Article

Effect of Curvature Shape on the Impact Strength of Additively Manufactured Acrylonitrile Butadiene Styrene Parts Produced via Fused Deposition Modeling

Muhammad Fahad *, Waseem Raja, Muhammad Naveed Iqbal * and Abdul Waheed Awan 

Department of Engineering, School of Digital, Technology, Innovation & Business, University of Staffordshire, Stoke-on-Trent ST4 2DE, UK; ww.raja001@gmail.com (W.R.); a.awan@staffs.ac.uk (A.W.A.)

* Correspondence: muhammad.fahad@staffs.ac.uk (M.F.); naveed.iqbal@staffs.ac.uk (M.N.I.)

Abstract: Additive manufacturing (AM) has greatly revolutionized manufacturing due to its ability to manufacture complex shapes without the need for additional tooling. Most AM applications are based on geometries comprising curved shapes subjected to impact loads. The main focus of this study was on investigating the influence of infill density and the radius of curvature on the impact strength of parts manufactured via an FDM process. Standard geometrical specimens with varying part infill densities and radii of curvature were produced and subjected to Charpy impact tests to evaluate their impact strength. The results suggest that the impact strength increases with the increased density caused by higher amounts of material as well as by the changing cross-sectional areas of the beads. Also, the radius of curvature of the parts shows a clear inverse relationship with the impact energy absorbed by the specimens (i.e., increasing the radius decreased the impact energy of the parts) produced via an FDM process, which can be explained using the beam theory of structural mechanics. The maximum value of impact strength obtained was 287 KJ/m², and this was achieved at the highest infill density (i.e., solid) and for the smallest radius of curvature.

Keywords: additive manufacturing; 3D printing; fused deposition modeling; acrylonitrile butadiene styrene; Charpy impact testing



Citation: Fahad, M.; Raja, W.; Iqbal, M.N.; Awan, A.W. Effect of Curvature Shape on the Impact Strength of Additively Manufactured Acrylonitrile Butadiene Styrene Parts Produced via Fused Deposition Modeling. *Designs* **2024**, *8*, 132. <https://doi.org/10.3390/designs8060132>

Academic Editor: Obeidi Muhannad

Received: 3 October 2024

Revised: 12 November 2024

Accepted: 22 November 2024

Published: 8 December 2024



Copyright: © 2024 by the authors. Licensee MDPI, Basel, Switzerland. This article is an open access article distributed under the terms and conditions of the Creative Commons Attribution (CC BY) license (<https://creativecommons.org/licenses/by/4.0/>).

1. Introduction

Scientific and technological progress during the twenty-first century has revolutionized modern living as well as manufacturing methods. One such revolution related to manufacturing processes is the advent of additive manufacturing (AM). Additive manufacturing, also known as three-dimensional (3D) printing, is the name given to a group of manufacturing processes which create parts contained in a digital file comprising the computer-aided design (CAD) data of the part [1]. The digital file contains information about the cross-sectional layers of the part at defined heights, and the machine used to produce this part extracts this information to create layers of material that are layered upon each other accordingly to create the geometry of the part. The manufacturing of components and shapes using AM techniques is performed without the need for any additional tooling, resulting in less product development time and fewer costs. At the same time, these processes provide various other advantages such as the consolidation of multiple parts into a single part, a complex design (design freedom), and the production of products with materials of different functional grades. Due to these advantages, three-dimensional printing processes have gained much attention during the last two decades and have shown applications in various industries, including the aerospace, automotive, home appliance, fashion, decoration, and biomedical sectors [1].

According to the ISO and ASTM, seven categories of additive manufacturing processes have been defined [2]. These categories are based on the type of technology used to produce a solid object and include technologies like powder sintering, photo-polymerization, inkjet

printing (binder or material), sheet lamination, electron-beam processing, and material extrusion. Material extrusion-based AM processes, commonly known as fused deposition modeling (FDM) or fused filament fabrication (FFF), are the main topics of this paper and will be explained further.

The process of FDM was introduced by Scott Crump [3] during the early 1990s and is based on extruding thin beads of molten thermoplastic material via a heated nozzle to form a layer of material. The nozzle typically moves in both the horizontal and vertical directions via a numerically controlled mechanism. The subsequent addition of layers results in a completed part. The process typically utilizes thermoplastic materials to build parts. Due to its relatively simple technical arrangement, extrusion-based 3D printing category is the most commonly utilized [4,5]. Commonly varied parameters during extrusion-based processes include the following [6–9]:

1. Layer thickness—the height of the deposited layer.
2. Infill density—the mass of the material within the volume of the geometry.
3. Infill patterns—the repetitive pattern of the beads deposited inside a layer.
4. Raster angle—the relative angle at which the beads are deposited within a single layer.
5. The orientation of the part—the relative placement of the part's CAD model within the build chamber.
6. Deposition speed—the relative speed of the extruding nozzle along the XY plane.
7. Build temperature—the temperature at which the material moves out of the nozzle.

Due to their wide variety of materials and their ability to produce complex shapes without needing additional tooling, extrusion-based AM processes have been widely adopted for short production runs (customized production) for a variety of applications [10,11], including automotive components [12,13], biomedical components [14], drug delivery [15], toys [16], energy storage devices [17], and personal protective equipment [18,19]. While extrusion-based AM can utilize numerous materials, acrylonitrile butadiene styrene (ABS) and polylactic acid (PLA) are the most frequently employed and studied materials [8,20–22]. For this research, ABS was chosen due to its superior mechanical properties. Consequently, the subsequent part of this literature review will focus primarily on ABS-related studies and applications.

The effect of varying printing parameters on the mechanical behavior of 3D-printed ABS parts has been discussed by different authors over the previous two decades. The research conducted and published by Fodran et al. [23] is one of the pioneering studies in this field. In their work, Fodran et al. investigated the influence of air gaps, the width, and the raster angle on the Young's modulus, the yield strength, and the tensile strength of parts. Similarly, another comprehensive study was performed by Sood et al. [8], who studied the effect of changing printing parameters on tensile strength. Their research highlighted that the tensile strength of the specimen initially decreased but then increased as the layer thickness increased. From this result, it can be anticipated that with a lower layer thickness, the number of layers will increase, which will result in a greater number of thermal cycles, which further leads to a higher temperature gradient within the previously stacked layers. This will increase the inter-raster and inter-layer bonding, and eventually, the strength of the part will improve. Other similar studies, such as those by Tymrak et al. [24] and Onwubolu et al. [25], indicated similar results. In other studies, Griffith et al. [26], Li et al. [27], Torres et al. [28] and Alafaghani et al. [29] have identified a visible correlation between the tensile strength of ABS parts and the infill density. All these studies suggest that an increase in infill density results in increased tensile strength for the 3D-printed parts. This increment in tensile strength is primarily attributed to the higher amount of material within the same volume. Therefore, parts with higher infill densities can endure higher loads and stresses without deforming or prior to fracturing. Therefore, these results clearly identify infill density as a very important factor in the design of 3D-printed objects for applications where mechanical strength is critical. However, increasing the infill density also increases both the amount of material required to print and the total time required to complete the part. This in turn, increases the total cost of part production at higher densities.

Similarly, the effect of process parameters on compressive strength has been studied comprehensively by many authors [30–35]. Ang K C et al. [30] studied the compressive strength by varying air gaps within 3D-printed parts of ABS and noted an increase in compressive strength upon reducing air gaps. Sood et al. [31] investigated the influence of layer thickness on the compressive behavior of ABS parts and showed that increasing layer thickness results in parts with higher compressive strength. The effect of varying the orientation of parts within the build chamber was studied by Hernandez et al. [32], and it was found that the compressive strength of parts built along the Z-plane was inferior to those built along the XY-plane. Dominguez-Rodríguez et al. [33] also evaluated the effect of build orientation along with different infill patterns on the compressive strength of 3D-printed ABS parts and showed that parts built along the vertical direction have a better compressive strength compared with the parts printed along the transverse direction. Recently, Fahad et al. [34] also studied the influence of process parameters such as part orientation, print density, and layer thickness on compressive strength and indicated that increasing layer thickness and print density have a direct effect on compressive strength.

Subsequent research has extensively explored the impact of process parameters on the mechanical properties of ABS parts. However, the majority of these studies focused primarily on tensile characteristics (such as the strength, elongation, and modulus of elasticity), with comparatively less attention given to impact behavior. Sood et al. [8] investigated the effects of layer thickness and part orientation, revealing that increased layer thickness led to higher impact energy absorption in parts. Notably, they found no significant variation in impact energy when changing part orientation within the XY-plane. Ziemian et al. [35] examined the influence of raster angle on impact behavior, observing a decrease in impact energy as the angle changed from 0° to 90°. Górski et al. [36] further explored part orientation, concluding that parts printed along the X-direction exhibited superior impact energy compared to other orientations. In a similar study, Dawoud et al. [37] investigated the effects of air gap and raster angle, determining that maximum strength was achieved with a raster angle of 45°. These findings collectively contribute to a growing body of knowledge on the relationship between process parameters and the mechanical properties of ABS parts produced through additive manufacturing.

Most of the parts produced via three-dimensional printing processes are complex in shape and comprise curved features. Specific examples of parts with curved shapes and features include helmets, masks, toys, medical implants, and automotive components. The presence of curved features not only influences the accuracy and surface finish but also affects the mechanical properties of the parts [38]. Also, most of the previously mentioned applications are typically subjected to impact loads, as opposed to other types of loads. Therefore, the objective of this study was to examine the influence of infill density and curved shape on the impact behavior of an ABS specimen produced via the fused deposition modeling process. Specimens with three different infill densities and varying radii of curvature were prepared and their impact strength was examined in order to evaluate their suitability for typical applications requiring curved-shaped parts printed via the FDM process.

2. Materials and Methods

2.1. Material

The material used to produce the test specimen in the study was Acrylonitrile Butadiene Styrene (ABS) plus material (filament diameter = 1.75 mm) manufactured by Stratasys (Edina, MN, USA). Important properties of the used material are indicated in Table 1. The material was used as received by the supplier without any further modifications.

Table 1. Printing parameters used in the research.

Property	Value	Unit
Yield Strength	31	MPa
Ultimate Tensile Strength	33	MPa
Elongation at Break	6%	-
Glass Transition Temperature	108	°C
Coefficient of thermal Expansion	8.82×10^{-5}	°C ⁻¹
Specific Gravity	1.04	-

2.2. Parts Printing

A uPrint SE FDM machine, manufactured and purchased by Stratasys (USA), was used to print the specimens. Three different infill densities, namely low, high, and solid, were used. The values of infill percentage were 53% at low, 81% at high, and 97% at solid. Three replicates of each type of specimen were produced, and the average results for each type were used to make a comparison. The parameters used to print the parts are indicated in Table 2. Parts were oriented during printing in the build chamber such that the length (L) was long on the x-axis, the width (W) was along y, the y-axis, and the thickness (T) was along z, the z-axis (Figure 1). The actual printed specimens are shown in Figure 2.

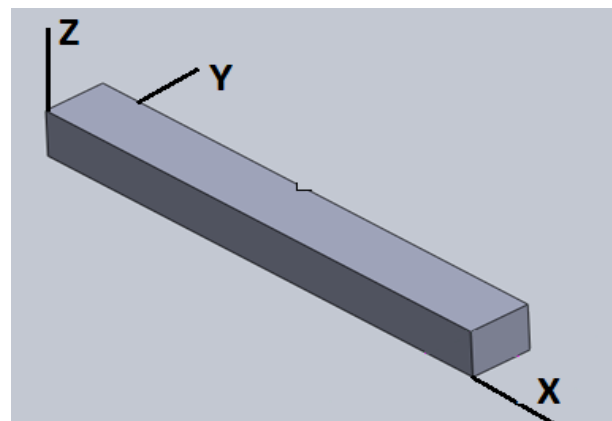


Figure 1. Part orientation within the build chamber during printing.

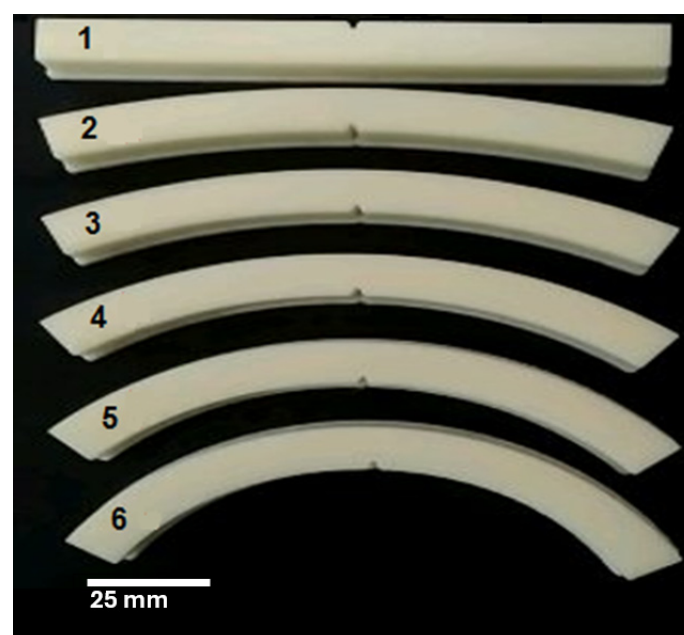


Figure 2. Six different types of specimens were printed for research.

Table 2. Printing parameters used in the research.

Parameter	Value	Unit
Nozzle Temperature	300	°C
Build Envelop Temperature	80	°C
Layer Thickness	0.254	mm
Nozzle diameter	0.4	mm
Raster Orientation	+45/−45	degrees

2.3. Impact Testing

Standard straight specimens for Charpy impact testing were produced according to ASTM D6110 [39] (Figure 3), where the length (L) was 127 mm, and the width (W) and the thickness (T) were 12.7 mm each. This straight sample was converted into a curved shape by changing the height (h) or radius of curvature (R) of a segment of the circle, as shown in Figure 3b. The cross-sectional area and the length of each specimen were kept constant to ensure that the overall volume remained constant. Six different specimen shapes (Figure 2), including one straight and five different curved shapes with a height (h) varying from 10 to 30 mm in increments of 5 mm, were used for building the specimen (Table 3). The impact strength was measured using the Charpy impact test. A pendulum impact energy tester G.U.N.T model WP-410 was used for the impact testing (Figure 4). The impact speed of the hammer was 5.5 m/s, and the total capacity of the hammer was 300 Nm. The impact energy was calculated by measuring the distance (d) traveled by the hammer after impact using the following equation, where m = mass of hammer, g = acceleration due to gravity, h = height of hammer, d = distance traveled by a hammer after impact and A = cross-sectional area of the specimen.

$$\text{Energy} = \text{Impact Strength} = mg(h - d)/A$$

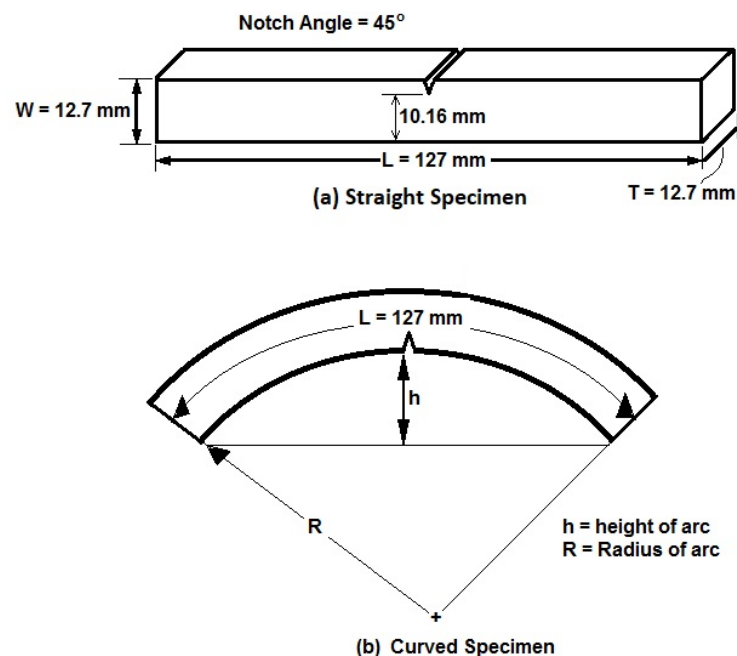


Figure 3. Dimensions of the impact specimens used in the research: (a) straight specimen; (b) curved specimen.

Table 3. Values of radius (R) and height (h) of the arc used in the research.

Part No.	Length of Arc (mm),	Radius of Arc (mm),	Height of Arc (mm),
	L	R	h
1	127	∞	0
2	127	199.92	10
3	127	131.82	15
4	127	97.27	20
5	127	76.04	25
6	127	61.42	30



Figure 4. Impact testing machine used in the research (GUNT WP410).

2.4. Scanning Electron Microscopy (SEM)

In order to analyze the cross-section of the broken samples after impact testing, Scanning Electron Microscopy (SEM) was used. Images were taken using analytical SEM by JEOL (Model Number: JSM-6380). The samples were sputtered with thin layers of gold using JEOL JFC-1500 sputtering equipment.

3. Results

As mentioned previously, six different samples were printed, with varying radii and heights of curvature (three replicates of each), as shown in Figure 2. The impact strength results were obtained by calculating the average of three samples of each type. The average values of each sample type are indicated in Table 4. Variations in impact strength with changes in infill density for different specimens are indicated in Figure 5, whereas Figure 6 shows the variations in impact strength with changes in the radius of curvature of specimens. Images of broken samples are shown in Figure 7.

Table 4. Average impact strength values for different specimens.

Infill Density → (g/cm ³)	Low 0.535				High 0.81				Solid 0.97				
	Part No. ↓	1	2	3	Avg.	1	2	3	Avg.	1	2	3	Avg.
1	1	31.14	31.6	31.46	31.4	52.39	53.62	52.6	52.9	118.32	119.1	117.78	118.4
	2	35.04	34.18	34.35	34.5	87.01	85.8	85.23	86.0	119.01	119.73	118.61	119.1

Table 4. Cont.

Infill Density → (g/cm ³)	Low 0.535				High 0.81				Solid 0.97				
	Part No. ↓	1	2	3	Avg.	1	2	3	Avg.	1	2	3	Avg.
	3	35.2	34.85	34.96	35.0	88.23	88.08	87.29	87.9	222.97	226.07	225.29	224.8
	4	38.7	38.97	38.93	38.9	113.89	114.98	115.43	114.8	283	280.68	278.95	280.9
	5	42.04	41.81	41.88	41.9	154.93	152.04	152.91	153.3	286.6	284.55	283.97	285.0
	6	125.64	124.12	123.2	124.3	254.32	256.57	256.12	255.7	287.8	286.41	286.88	287.0

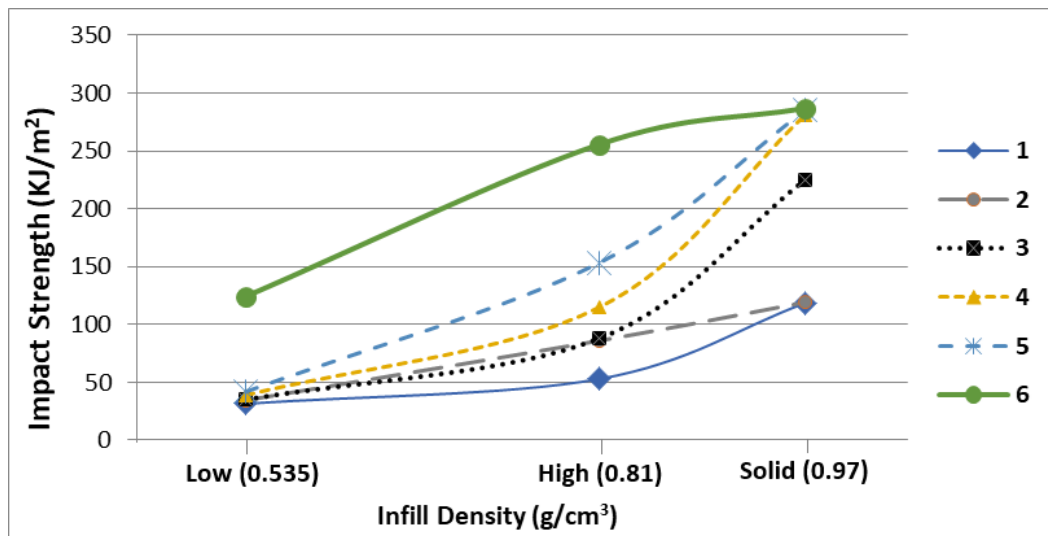


Figure 5. Variation in impact strength with print density.

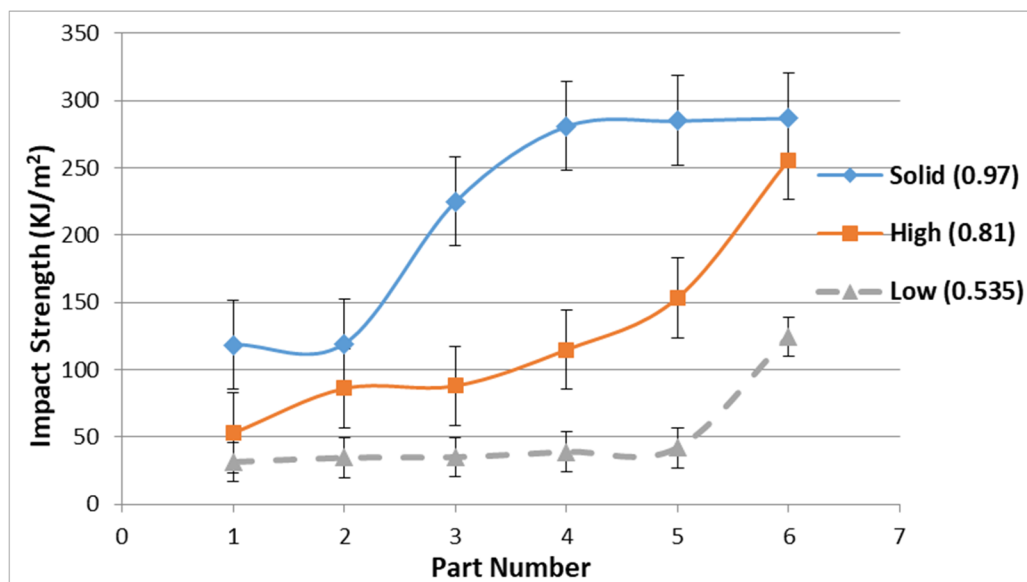


Figure 6. Variation in impact strength with part curvature.

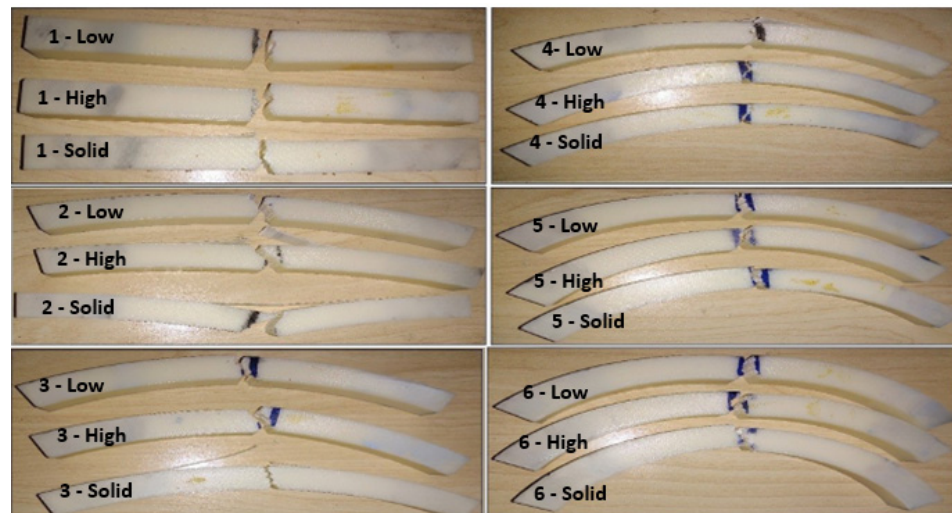


Figure 7. Images of samples after impact testing.

4. Discussion

4.1. Effect of Infill Density

Unlike most available open-source 3D printers, the 3D printer used in this research did not allow the print density to be set at any quantitative value. Rather, three options, low, high, and solid, could be selected to build parts. Therefore, to find the actual value of infill density, the mass of parts printed at different densities was measured and divided by the volume (constant for all parts) to obtain the actual density values for the three levels. These values were found to be 0.535 g/cm^3 , 0.81 g/cm^3 , and 0.97 g/cm^3 for low, high, and solid densities, respectively. The variation in impact strength with print density is shown in Figure 5, and it is evident that the impact strength increased with the increase in print density. It was shown previously that increasing print density results in increased tensile strength and impact strength [34,37,40]. This can be attributed to the close packing of material inside the same volume at higher print densities, resulting in more energy being required for fracture. A scanning electron microscopy (SEM) of the fractured specimen was conducted, and the results are indicated in Figures 8 and 9. Both Figures 8 and 9 clearly indicate that the material failed under the brittle fracture mode, and this is consistent with the material behavior defined by the manufacturer (only 6% elongation at break) in Table 1. It is clear from Figures 8a and 9a that for the lowest-density sample, more empty spaces are present, and these void spaces act as pre-existing cracks to initiate fracture. On the other hand, for the high-density (Figures 8b and 9b) and solid-density samples (Figures 8c and 9c), the internal structure is much more compact and contains very few empty spaces. The decrease in the presence of crack-initiating points results in a higher impact energy requirement for the fracture of parts with increased infill density. It is also evident from Figures 8 and 9 that the shape of the beads in lower-density samples is consistently circular. For the highest-density (i.e., solid) samples, the circular bead shape changes to an elliptical shape. It is well known in mechanics that, for the same cross-sectional area, the elliptical shape has a higher moment of inertia along the major axis (the axis along the width of the bead) compared to the moment of inertia of the circular cross-section [41,42]. This higher moment of inertia also strengthens the internal structure and results in higher energy absorption before fracture as the density of the specimen is increased. It may be noted that the high amount of material that is present mainly causes this change in the cross-sectional shape of beads in higher-density specimens with the same volume (i.e., a high infill density). The excess weight presses the previously deposited beads into an elliptical shape. On the other hand, for low-density samples, the amount of material on top of the beads is not sufficiently large to cause this elliptic deformation.

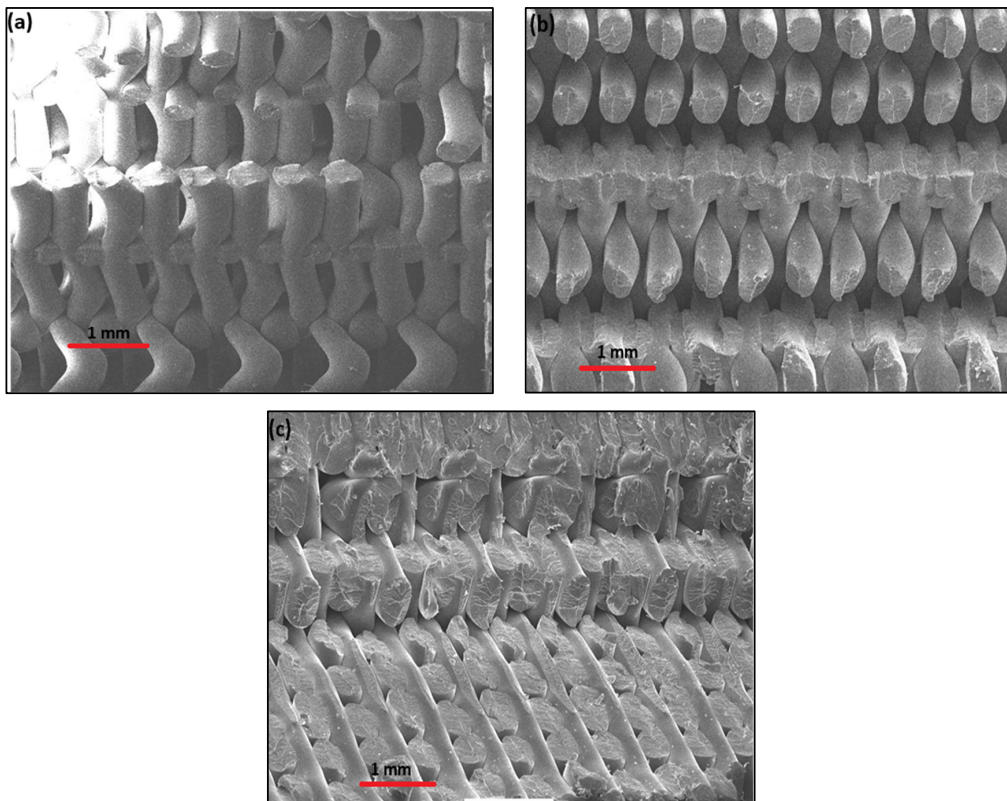


Figure 8. SEM images of part 1 (0 mm height of arc) at: (a) low density; (b) high density; (c) solid density.

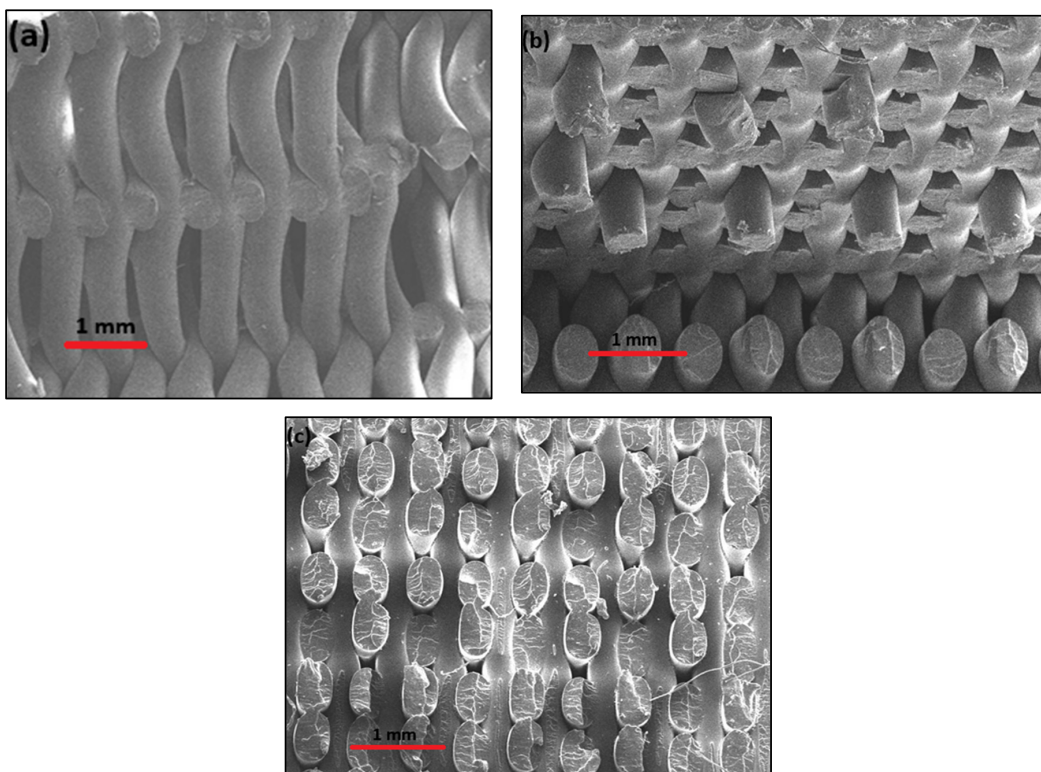


Figure 9. SEM images of part 6 (30 mm height of arc) at a (a) low density, (b) high density, and (c) solid density.

4.2. Effect of Curvature

The trend of impact strength changing with the changing radius of curvature at each infill density is presented in Figure 6, and it is clear that decreasing the radius of curvature (indicated by increasing part number) at a fixed infill density results in increased impact energy for samples of all densities. Although no study related to curved 3D-printed structures is available, curved composite structures have been subjected to impact loads, and similar results were achieved [43,44]. The reason behind this increased impact strength can be explained using the commonly used bending stress equation for curved beams (Figure 10), as presented in Equation (1), where σ_b = bending stress; E = Young's modulus; y = distance (from neutral axis) of the layer subjected to bending; R = radius of curvature:

$$\sigma_b = \frac{E \cdot y}{R}, \tag{1}$$

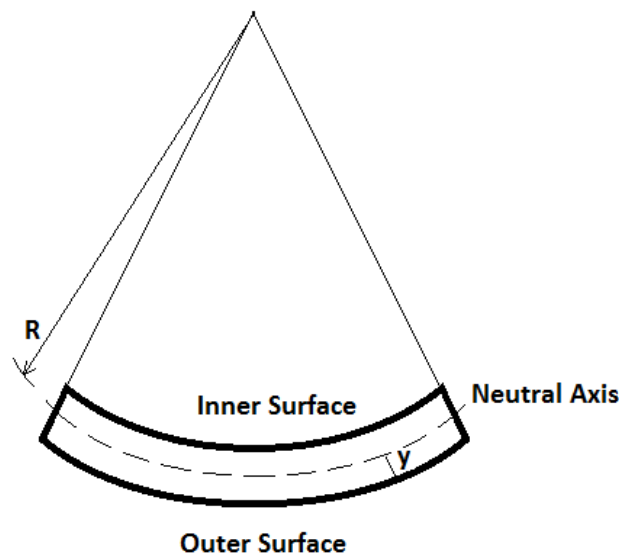


Figure 10. Schematic diagram of a curved beam.

Curved beams have an internal moment or bending moment, which is composed of tensile and compressive stresses at their outer surfaces, as given by Equation (1). This means that the outer surface of the curved specimen is under tensile stress, and the inner side is under compressive stress. When the impact load is applied on the outer surface of the curved specimen, the presence of tensile stress results in an increase in the amount of energy needed to fracture the specimen. As the radius of the arc (i.e., R) is decreased from samples 1 to 6, the bending stresses increase, and therefore, the energy required to break the specimen increases from samples 1 to 6.

However, it is clear from Figure 6 that a sharp rise in impact energy occurred in the highest-density samples at relatively higher radius values (i.e., a sharp rise between parts 2 and 3). This indicates that for higher-density samples, the impact strength for a relatively low depth of curvature is also high. This may be attributed to the fact that at a solid density, the beads within the cross-section are very tightly packed. However, increasing the curvature (reduced radius of curvature) causes the voids, which act as crack initiation points, to come closer; therefore, a sharp rise in impact strength takes place between parts 3 and 4. Therefore, printing parts at a higher density can provide good a impact strength even at relatively high or arc values. An appreciable rise in impact strength for low-density samples was obtained at a low arc radius (increased depth). This means when printing parts at a low density, to obtain a suitable impact strength, a smaller radius of curvature would be preferred. This may be because, at low densities, the voids acting as crack initiation points move closer at a small radius of curvature, as indicated by Figures 8a and 9a. On the other hand, the samples printed with medium density values (i.e., 0.81 g/cm^3) showed a

nearly linear behavior of increasing impact strength at reduced radius values for the arc. This may be because the compactness of the voids remains consistent at all curvatures for samples with a density between low and solid. This implies that a medium-print density is more suited for the entire arc radius range.

These results show that the use of the FDM process for producing end-use items containing curved shapes (helmets, masks, medical implants, etc.) is beneficial in the sense that these parts have increased strength and are able to withstand higher impact loads than parts with flat shapes. The results of this study can help users of commercial FDM processes to produce curved parts by selecting appropriate curve radii values within their part design and identifying the appropriate infill density. Selecting the right curve radius will ensure that the part is produced with the desired impact strength, making it suitable for its end application. Additionally, the selection of an appropriate infill density will help in the manufacturing of parts by ensuring an appropriate amount of material and an appropriate printing time are used. The printing time and the amount of material required to print parts are directly linked to the cost and overall environmental impact of additive manufacturing. Therefore, these results provide users with suitable values for the infill density and suitable curvature values to ensure that the target strength is achieved while ensuring minimal costs and a minimal environmental impact. These results can help when using the FDM process to build parts for applications that require curved-shape components. These applications include toy manufacturing, automotive parts, biomedical components, jewelry items, and home appliances.

5. Conclusions

Specimens with varying print densities and curvature were manufactured using ABS material using a fused deposition modeling process. The printed specimens were subjected to Charpy impact testing to evaluate the influence of infill density and the radius of curvature on the impact strength. The main findings of the study are as follows:

- The results indicate that the impact strength increased upon increasing the infill density for all parts due to the increased amount of material inside an identical volume. This is consistent with the literature. The main reason behind this increase is the close packing of material inside the cross-section.
- SEM results indicated a change in bead shape from circular to elliptical upon increasing infill density. This change in bead shape also helps increase energy absorption before fracture.
- The results further showed that decreasing the arc radius resulted in an increased impact strength of the parts at all densities.

This increased impact strength shows that the FDM technique is suitable for producing different curved-shaped end-use items such as helmets, toys, masks, and automotive components. The results can help users of the FDM process in selecting an appropriate combination of infill density and curve radii to ensure the correct amount of material and print time are selected for printing parts while achieving the desired impact strength.

Author Contributions: Conceptualization, M.F. and W.R.; methodology, M.F., M.N.I. and W.R.; software, W.R., M.N.I. and A.W.A.; validation, M.F. and A.W.A.; formal analysis, A.W.A., M.N.I. and W.R.; writing—original draft preparation, M.F. and W.R.; writing—review and editing, M.N.I. and A.W.A.; visualization, A.W.A. and M.N.I.; supervision, M.F. All authors have read and agreed to the published version of the manuscript.

Funding: This research received no external funding.

Data Availability Statement: Data are contained within the article.

Acknowledgments: Authors acknowledge Karachi University for providing support during scanning electron microscopy of the samples.

Conflicts of Interest: The authors declare no conflicts of interest.

References

1. Fahad, M. Additive Manufacturing. In *Foundations of Materials Science and Engineering*; Trans Tech Publications: Stafa-Zurich, Switzerland, 2017; Volume 93, pp. 355–376.
2. *ISO/ASTM 52900; Additive Manufacturing—General Principles—Terminology*. International Organization for Standardization: Geneva, Switzerland, 2015.
3. Crump, S.S. Apparatus and Method for Creating Three-Dimensional Objects. U.S. Patent US 5121329 A, 9 June 1992.
4. Tessa, J.G.; Philipp, R.T.; Louis, T.; Lars, J. Optimising the FDM additive manufacturing process to achieve maximum tensile strength: A state-of-the-art review. *Rapid Prototyp. J.* **2019**, *25*, 953–971.
5. Andrei, D.M.; Dumitru, N.; Ramona, P. Additive manufacturing of composite materials by FDM technology: A review. *Indian J. Eng. Mater. Sci.* **2019**, *27*, 179–192.
6. Popescu, D.; Zapciu, A.; Amza, C.; Baciuc, F.; Marinescu, R. FDM process parameters influence over the mechanical properties of polymer specimens: A review. *Polym. Test.* **2018**, *69*, 157–166. [[CrossRef](#)]
7. Montero, M.; Roundy, S.; Odell, D.; Ahn, S.H.; Wright, P.K. Material characterization of fused deposition modeling (FDM) ABS by designed experiments. *Soc. Manuf. Eng.* **2001**, *10*, 1–21.
8. Sood, A.K.; Ohdar, R.K.; Mahapatra, S.S. Parametric appraisal of mechanical property of fused deposition modelling processed parts. *Mater. Des.* **2010**, *31*, 287–295. [[CrossRef](#)]
9. Madan, M.N.; Harshvardhan, G.K.; Biradar, D.M. An Overview: Fused Deposition Modeling Process. *J. Emerg. Technol. Innov. Res.* **2020**, *7*, 2115–2119.
10. Whelan, C.; Sheahan, C. Using additive manufacturing to produce injection moulds suitable for short series production. *Procedia Manuf.* **2019**, *38*, 60–68. [[CrossRef](#)]
11. Roberson, D.; Shemelya, C.M.; MacDonald, E.; Wicker, R. Expanding the applicability of FDM-type technologies through materials development. *Rapid Prototyp. J.* **2015**, *21*, 137–143. [[CrossRef](#)]
12. Romero, P.E.; Arribas-Barrios, J.; Rodriguez-Alabanda, O.; González-Merino, R.; Guerrero-Vaca, G. Manufacture of polyurethane foam parts for automotive industry using FDM 3D printed molds. *CIRP J. Manuf. Sci. Technol.* **2021**, *32*, 396–404. [[CrossRef](#)]
13. Maurya, N.K.; Rastogi, V.; Singh, P. Comparative study and measurement of form errors for the component printed by FDM and PolyJet process. *Instrum. Mes. Métrologie* **2019**, *18*, 353–359. [[CrossRef](#)]
14. Singh, D.; Singh, R.; Boparai, K.S. Development and surface improvement of FDM pattern based investment casting of biomedical implants: A state of art review. *J. Manuf. Process.* **2018**, *31*, 80–95. [[CrossRef](#)]
15. Linares, V.; Casas, M.; Caraballo, I. Printfills: 3D printed systems combining fused deposition modeling and injection volume filling. Application to colon-specific drug delivery. *Eur. J. Pharm. Biopharm.* **2019**, *134*, 138–143. [[CrossRef](#)] [[PubMed](#)]
16. León-Cabezas, M.A.; Martínez-García, A.; Varela-Gandía, F.J. Innovative functionalized monofilaments for 3D printing using fused deposition modeling for the toy industry. *Procedia Manuf.* **2017**, *13*, 738–745. [[CrossRef](#)]
17. Chang, P.; Mei, H.; Zhou, S.; Dassios, K.G.; Cheng, L. 3D printed electrochemical energy storage devices. *J. Mater. Chem. A* **2019**, *7*, 4230–4258. [[CrossRef](#)]
18. Wang, P.; Yang, J.; Hu, Y.; Huo, J.; Feng, X. Innovative design of a helmet based on reverse engineering and 3D printing. *Alex. Eng. J.* **2021**, *60*, 3445–3453. [[CrossRef](#)]
19. Jafferson, J.M.; Pattanashetti, S. Use of 3D printing in production of personal protective equipment (PPE)—A review. *Mater. Today Proc.* **2021**, *46*, 1247–1260. [[CrossRef](#)]
20. Novakova-Marcincinova, L.; Novak-Marcincin, J. Testing of materials for rapid prototyping fused deposition modelling technology. *Int. J. Ind. Manuf. Eng.* **2012**, *6*, 2082–2085.
21. Novakova-Marcincinova, L.; Novak-Marcincin, J. Applications of rapid prototyping fused deposition modeling materials. In *Annals of DAAAM for 2012 & Proceedings of the 23rd International DAAAM Symposium 2012*; AAAM International: Vienna, Austria, 2012; Volume 23, pp. 57–60.
22. Lay, M.; Thajudin, N.L.; Hamid, Z.A.; Rusli, A.; Abdullah, M.K.; Shuib, R.K. Comparison of physical and mechanical properties of PLA, ABS and nylon 6 fabricated using fused deposition modeling and injection molding. *Compos. Part B Eng.* **2019**, *176*, 107341. [[CrossRef](#)]
23. Fodran, E.; Koch, M.; Menon, U. Mechanical and dimensional characteristics of fused deposition modeling build styles. In *Proceedings of the Solid Freeform Fabrication Proceedings*, Austin, TX, USA, 12–14 August 1996; pp. 419–442.
24. Tymrak, B.M.; Kreiger, M.; Pearce, J.M. Mechanical properties of components fabricated with open-source 3-D printers under realistic environmental conditions. *Mater. Des.* **2014**, *58*, 242–246. [[CrossRef](#)]
25. Onwubolu, G.C.; Rayegani, F. Characterization and Optimization of Mechanical Properties of ABS Parts Manufactured by the Fused Deposition Modeling Process. *Int. J. Manuf. Eng.* **2014**, *2014*, 598531. [[CrossRef](#)]
26. Griffiths, C.A.; Howarth, J.; Rowbotham, G.d.-A.; Rees, A. Effect of Build Parameters on Processing Efficiency and Material Performance in Fused Deposition Modelling. *Procedia CIRP* **2016**, *49*, 28–32. [[CrossRef](#)]
27. Li, H.; Wang, T.; Sun, J.; Yu, Z. The effect of process parameters in fused deposition modelling on bonding degree and mechanical properties. *Rapid Prototyp. J.* **2018**, *24*, 80–92. [[CrossRef](#)]
28. Torres, J.; Cole, M.; Owji, A.; DeMastry, Z.; Gordon, A.P. An approach for mechanical property optimization of fused deposition modeling with polylactic acid via design of experiments. *Rapid Prototyp. J.* **2016**, *22*, 387–404. [[CrossRef](#)]

29. Alafaghani, A.; Qattawi, A.; Alrawi, B.; Guzman, A. Experimental Optimization of Fused Deposition Modelling Processing Parameters: A Design-for-Manufacturing Approach. *Procedia Manuf.* **2017**, *10*, 791–803. [CrossRef]
30. Ang, K.C.; Leong, K.F.; Chua, C.K. Chandrasekaran M. Investigation of the mechanical properties and porosity relationships in fused deposition modeling-fabricated porous structures. *Rapid Prototyp. J.* **2006**, *12*, 100–105.
31. Sood, A.K.; Ohdar, R.K.; Mahapatra, S.S. Experimental investigation and empirical modeling of FDM process for compressive strength improvement. *J. Adv. Res.* **2011**, *3*, 81–90. [CrossRef]
32. Hernandez, R.; Slaughter, D.; Whaley, D.; Tate, J.; Asiabanpour, B. Analyzing the tensile, compressive, and flexural properties of 3D printed ABS P430 plastic based on printing orientation using fused deposition modeling. In Proceedings of the Solid Freeform Fabrication 2016: Proceedings of the 26th Annual International Solid Freeform Fabrication Symposium, Austin, TX, USA, 8–10 August 2016; pp. 939–950.
33. Domínguez-Rodríguez, G.; Ku-Herrera, J.J.; Hernández-Pérez, A. An assessment of the effect of printing orientation, density, and filler pattern on the compressive performance of 3D printed ABS structures by fuse deposition. *Int. J. Adv. Manuf. Technol.* **2018**, *95*, 1685–1695. [CrossRef]
34. Fahad, M.; Mujeeb, M.; Khan, M.A. Effect of Process Parameters on the Compressive and Impact Strength of 3D Printed Parts. *Iran. J. Sci. Technol. Trans. Mech. Eng.* **2022**, *47*, 257–265. [CrossRef]
35. Ziemian, C.; Sharma, M.; Ziemian, S. Anisotropic mechanical properties of ABS parts fabricated by fused deposition modelling. *Mech. Eng.* **2012**, *23*, 159–180.
36. Górski, F.; Wichniarek, R.; Kuczko, W.; Zawadzki, P.; Buń, P. Strength of ABS parts produced by Fused Deposition Modelling technology—a critical orientation problem. *Adv. Sci. Technol. Res. J.* **2015**, *9*, 12–19. [CrossRef]
37. Dawoud, M.; Taha, I.; Ebeid, S.J. Mechanical behaviour of ABS: An experimental study using FDM and injection moulding techniques. *J. Manuf. Process.* **2016**, *21*, 39–45. [CrossRef]
38. Huang, B.; Singamneni, S. Alternate slicing and deposition strategies for fused deposition modelling of light curved parts. *J. Achiev. Mater. Manuf. Eng.* **2012**, *55*, 511–517.
39. Fernandez-Vicente, M.; Calle, W.; Ferrandiz, S.; Conejero, A. Effect of infill parameters on tensile mechanical behavior in desktop 3D printing. *3D Print. Addit. Manuf.* **2016**, *3*, 183–192. [CrossRef]
40. Rodríguez-Panes, A.; Claver, J.; Camacho, A.M. The influence of manufacturing parameters on the mechanical behaviour of PLA and ABS pieces manufactured by FDM: A comparative analysis. *Materials* **2018**, *11*, 1333. [CrossRef]
41. Moment of Inertia—Elliptical Beam. Available online: <https://www.physicsforums.com/threads/moment-of-inertia-elliptical-beam.244049> (accessed on 15 September 2024).
42. Pope, J.E. *Rules of Thumb for Mechanical Engineers*; Gulf Pub. Co.: Houston, TX, USA, 1997.
43. Saghafi, H.; Minak, G.; Zucchelli, A. Effect of preload on the impact response of curved composite panels. *Compos. Part B Eng.* **2014**, *60*, 74–81. [CrossRef]
44. Baba, B.O. Curved sandwich composites with layer-wise graded cores under impact loads. *Compos. Struct.* **2017**, *159*, 1–11. [CrossRef]

Disclaimer/Publisher’s Note: The statements, opinions and data contained in all publications are solely those of the individual author(s) and contributor(s) and not of MDPI and/or the editor(s). MDPI and/or the editor(s) disclaim responsibility for any injury to people or property resulting from any ideas, methods, instructions or products referred to in the content.